HAL
open science

Distinguishing Mesoscale Polar Order (Unidirectional vs Bidirectional) of Cellulose Microfibrils in Plant Cell Walls Using Sum Frequency Generation Spectroscopy

Mohamadamin Makarem, Yoshiharu Nishiyama, Xiaoran Xin, Daniel Durachko, Ying Gu, Daniel J Cosgrove, Seong H Kim

To cite this version:

Mohamadamin Makarem, Yoshiharu Nishiyama, Xiaoran Xin, Daniel Durachko, Ying Gu, et al.. Distinguishing Mesoscale Polar Order (Unidirectional vs Bidirectional) of Cellulose Microfibrils in Plant Cell Walls Using Sum Frequency Generation Spectroscopy. Journal of Physical Chemistry B, 2020, 124 (37), pp.8071-8081. 10.1021/acs.jpcb.0c07076 . hal-02951273

HAL Id: hal-02951273

https://hal.science/hal-02951273v1

Submitted on 12 Oct 2021

HAL is a multi-disciplinary open access archive for the deposit and dissemination of scientific research documents, whether they are published or not. The documents may come from teaching and research institutions in France or abroad, or from public or private research centers.

L'archive ouverte pluridisciplinaire **HAL**, est destinée au dépôt et à la diffusion de documents scientifiques de niveau recherche, publiés ou non, émanant des établissements d'enseignement et de recherche français ou étrangers, des laboratoires publics ou privés.

Distinguishing Mesoscale Polar Order (Unidirectional vs. Bidirectional) of Cellulose Microfibrils in Plant Cell Walls using Sum Frequency Generation Spectroscopy

Mohamadamin Makarem[1], Yoshiharu Nishiyama[2], Xiaoran Xin[3], Daniel Durachko[4], Ying Gu[3], Daniel J. Cosgrove[4], and Seong H. Kim[1*]

[1] Department of Chemical Engineering, Materials Research Institute, Pennsylvania State University, University Park, Pennsylvania 16802, USA.

[2] University Grenoble Alpes, CNRS, CERMAV, 38000 Grenoble, France.

[3] Department of Biochemistry and Molecular Biology, Pennsylvania State University, University Park, Pennsylvania 16802, USA.

[4] Department of Biology, Pennsylvania State University, University Park, Pennsylvania 16802, USA.

* Corresponding author: shkim@engr.psu.edu, shk10@psu.edu.

TOC Figure

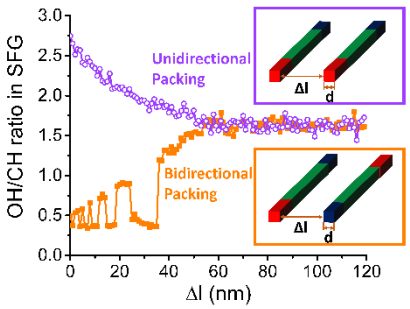

Abstract

Cellulose in plant cell walls is crystalline microfibrils with diameters of 3~4 nm and lengths of around 1-10 μm. These microfibrils are known to be the backbone of cell walls, and their multiscale three-dimensional organization plays critical role in cell wall functions including plant growth and recalcitrance to degradation. The mesoscale organization of microfibrils over a 1 – 100 nm range in cell walls is challenging to resolve because most characterization techniques investigating this length scale suffer from low spatial resolution, sample preparation artifacts, or inaccessibility of specific cell types. Here we report a sum frequency generation (SFG) study determining the mesoscale polarity of cellulose microfibrils in intact plant cell walls. SFG is a non-linear optical spectroscopy technique sensitive to the molecular-to-mesoscale order of non-centrosymmetric domains in amorphous matrices. However, the quantitative theoretical model to unravel the effect of polarity in packing of non-centrosymmetric domains on SFG spectral features has remained unresolved. In this work, we show how the phase synchronization principle of the SFG process is used to predict the relative intensities of vibrational modes with different polar angles from the non-centrosymmetric domain axis. Applying this model calculation for the first time and employing SFG microscopy, we found that cellulose microfibrils in certain xylem cell walls are deposited unidirectionally (or biased in one direction), instead of the bidirectional polarity which was believed to be dominant in plant cell walls from volume-averaged characterizations of macroscopic samples. With this advancement in SFG analysis, one can now determine the relative polarity of non-centrosymmetric domains such as crystalline biopolymers interspersed in amorphous polymer matrices, which will open opportunities to study new questions that have not been conceived in the past.

Introduction

In plants, cell walls consist of cellulose microfibrils (CMFs) and various types of polysaccharides. The elementary CMFs are synthesized and deposited by the cellulose synthase complexes (CSCs) moving in the plasma membrane of the cell.[1-2] In each elementary CMF, the directionality of β-1→4 glycosidic bonds from the reducing end to the non-reducing end is the same for all chains.[1] Thus, the spatial arrangement as well as the overall directionality of CMFs in plant cell walls can provide the information about the spatial distribution and movement of CSCs in the cell membrane during the CMF synthesis, which is directly coupled with the biological and mechanical function of the cells in various tissues in plants.[3-6] The cellulose structures also play a critical role in the recalcitrance of lignocellulosic biomass in enzymatic and chemical conversion to other useful forms of chemicals.[7-9]

Plant cell walls are divided into two types – a primary cell wall (PCW) which can expand during the growth of the cell and a secondary cell wall (SCW) which undergoes wall thickening after cell growth and expansion have ceased.[10] In the PCW, CSCs are mostly isolated and move individually along the microtubules beneath the cell wall.[11] Based on the literature reported so far, the CSCs in PCWs move bi-directionally with almost equal probabilities of the opposite directions of the microtubule.[12] PCWs have a crossed-polylamellate structure; in each lamella, CMFs are deposited along a dominant direction with some local variances and the dominant direction varies from lamella to lamella.[13] Many experimental evidences suggest that CSCs in SCWs move collectively in clusters or certain geometric arrays.[10, 14-16] SCWs are usually composed of S1, S2, and S3 layers.[15] Among these, the S2 layers are normally the thickest and the CMFs in the S2 layer are highly aligned at a specific angle, called with microfibril angle (MFA), with respect to the longitudinal axis of the cell.[17] If the CSCs in SCWs also move bi-

directionally along the microtubules (Figure 1a), the CMFs would have the bidirectional packing, in average, along the MFA axis. However, it was recently reported that in the xylem cell wall induced in the epidermis of Arabidopsis hypocotyl, the CSC movements can be preferentially unidirectional (biased toward one direction of the cortical microtubule over the other direction, as shown in Figure 1b).[12] This would result in the partially unidirectional deposition of CMFs in the cell wall. The degree of unidirectionality or deviation from the bidirectionality of CMFs in SCWs will be directly related to the preferential CSC movement along one direction over the other during the cellulose synthesis in plant cell walls. Thus, if one can distinguish the unidirectional versus bidirectional deposition of the CMFs in the cell wall, it would be possible to infer the directionality of the CSC movement during the CMF synthesis and deposition.

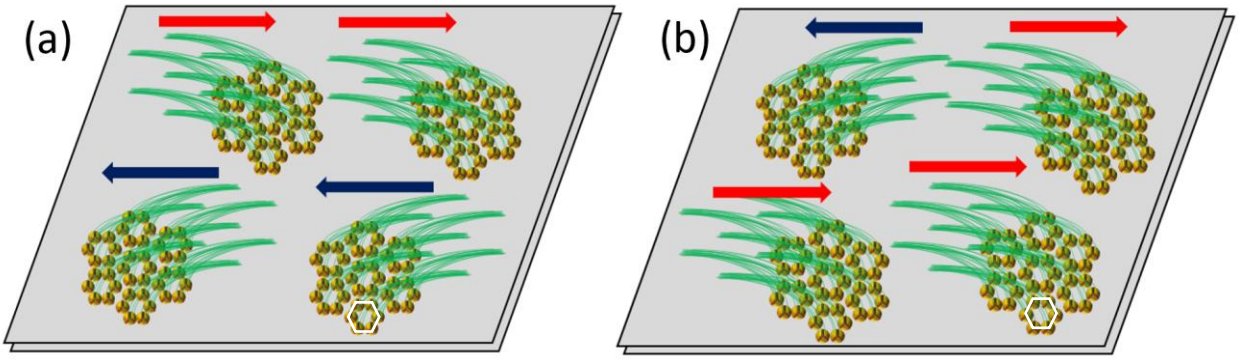

Figure 1. Schematic illustration of two possible movement directionalities of CSCs – (a) equal probability for two opposite directions along the microtubule axis and (b) preferential direction along one direction over the other. This image is drawn with the hexagonal arrays of rosette-shape CSCs (marked with hexagon-shape outlines) observed in electron microscopy imaging of the SCW of a unicellular green alga *Micrasterias*.[18] Cellulose chains extruded from each rosette-shape CSCs are assembled into elementary CMFs which can be bundled into macrofibrils.

Various analytical techniques have been employed for structural analyses of cellulose in plant cell walls; these include x-ray diffraction (XRD), x-ray or neutron scattering, nuclear magnetic resonance (NMR), and vibrational spectroscopy such as infrared (IR), Raman, and sum

frequency generation (SFG). Diffraction and scattering techniques can reveal the recurring structural order of CMFs from sub-nm to mesoscales (1 – 100 nm),[19-23] but they cannot determine the directionality of CMFs. NMR can probe molecular conformations of cellulose and dynamic interactions with other matrix polymers in plant cell walls,[24-27] but it cannot provide the information on the directionality of CMFs. IR and Raman spectroscopy often suffer from spectral interferences from non-cellulosic polymers co-present in plant cell walls.[28-31] In contrast, SFG is proven to be sensitive to crystalline cellulose only in the plant cell walls.[32-34] This cellulose-specificity originates from the non-centrosymmetry requirement of the nonlinear optical process.[35-38] In the plant cell wall, the crystalline cellulose is the only component meeting this requirement and other amorphous polysaccharides cannot produce SFG signals.[32] In this paper, we demonstrate that the same non-centrosymmetry requirement can be combined with the SFG phase synchronization principle to determine the overall directionality of the CMFs in plant cell walls.

The proof of concept for this approach was originally suggested by recent time-dependent density functional theory (TD-DFT) calculations predicting SFG spectral features for uniaxially-aligned cellulose crystallites in unidirectional and bidirectional packing.[39] Figure 2 schematically illustrates two cellulose crystals (represented with square rods) separated by a given distance, Δl, and the TD-DFT calculation results for the unidirectional and bidirectional packing cases with Δl = 0 (intimate contact). The transition dipole moments of the SFG-active OH stretch modes are in the (200) plane of the cellulose Iβ unit cell with specific tilt angles from the chain axis.[30, 39-40] In contrast, the transition dipole moments of the SFG-active CH and CH_2 stretch modes are off the (200) plane. Thus, the OH dipoles can be enhanced when two crystallites are unidirectional (parallel) and cancelled when one crystallite is rotated by 180° along the a-axis of the unit cell,

making two crystallites bidirectional (antiparallel) to each other. In contrast, such cancellation effects for the same rotation are weaker for the CH dipoles. For this reason, the OH SFG peak is predicted to be larger than the CH SFG peak for the unidirectional-packed crystals (Figure 2c) and smaller for the bidirectional-packed crystals (Figure 2d). Here, the degree of enhancement or cancellation effects depends on the degree of phase matching between SFG signals of adjacent crystallites which is in turn a function of the inter-crystallite distance, Δl.

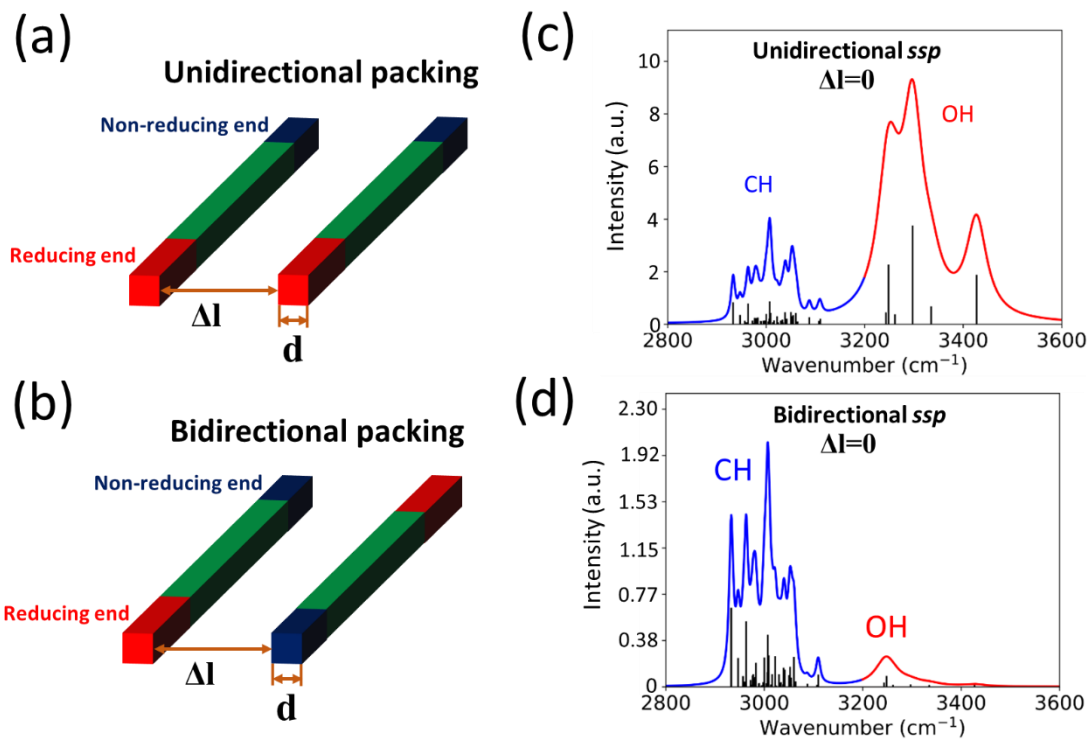

Figure 2. Schematic illustration of two cellulose crystallites in (a) unidirectional and (b) bidirectional packing and TD-DFT prediction of SFG spectral features for two crystals in intimate contact with (c) unidirectional and (d) bidirectional packing. The calculations were for crystalline domains consisting of cellobiose units with atomic positions in the cellulose Iβ coordinate. Note that the y-scale of the bidirectional packing case (d) is about 4 times smaller than the unidirectional case (c).[30, 39]

This paper explains how the phase synchronization function can be used to predict the SFG intensities of the CH and OH stretching modes of cellulose using the transition dipole

moments determined from TD-DFT. The theoretical calculations in this paper are for the uniaxially aligned cellulose crystallites in relevance to the CMFs in SCWs. Then, we confirm the theoretical predictions for the bidirectional case using a well-controlled model system consisting of the cellulose nanocrystals (CNCs) suspended in D_2O at different concentrations and placed in a capillary tube. This model system provides equally-spaced, uniaxially-aligned CNCs without preferential directionality (so, equivalent to the bidirectional polarity in average). Finally, we employ the theoretically predicted OH/CH SFG intensity ratio to argue that CMFs in two xylem-type walls have the unidirectional polarity, which is quite unexpected considering that the volume-averaged SFG signals of many SCW samples indicates that bidirectional CMFs are dominant.[41]

Methods

Cellulose nanocrystal suspension solutions

The tunicate mantle of tunicate (Halocynthia roretzi), kindly provided Okasei Ltd. (Onagawa, Japan) was used as starting material. After purification by alternating treatment by alkali and sodium chlorite, the samples were cut to strips about 2 mm wide, and treated with double cylinder type homogenizer in water. The resulting slurry was centrifuged to remove excess water, and hydrolyzed in 50% sulfuric acid at 55˚C at solid content of 1-2% for 20 hours under continuous agitation PTFE coated propeller. After removal of most of sulfuric acid by centrifugation at 20,000 g, the sample was repeatedly diluted and centrifuged at about 3000 g for 20 min with the transparent supernatant discarded. After several cycles of the slow speed centrifugation wash, the supernatant start to contain colloidal particles with milky appearance. This supernatant was harvested by centrifugation at 20,000 g for 1 hour. This operation was

repeated until no colloidal particle left floating, leaving acid resistant agglomerates in the slow centrifugation step. The colloidal particle was further washed with repeated centrifugation at 20,000 g for 8 hours, and dilution with deionized water until the electric conductivity of the suspension was below 100 µS/cm. The counter ion of sulfate group was then exchanged to sodium by adding dilute NaOH solution and sonicated at about 1% solid content using an ultrasonic homogenizer until the temperature of water raised by about 20 ˚C. The water was exchanged to heavy water again by repeated centrifugation and dilution using 99.9% D_2O. The suspension at 4% was then kept as mother solution and diluted with D_2O to prepare different concentration.

Arabidopsis hypocotyls

We generated *Arabidopsis* transgenic plants expressing a master regulator of xylem differentiation, Vascular-related NAC-domain 7, fused to a glucocorticoid receptor (35S::VND7-GR).[12] *Arabidopsis* seeds were surface sterilized with 30% (vol/vol) bleach for 15 min, thoroughly washed with autoclaved double-distilled H_2O (ddH_2O), and stored at 4 °C for 3 days. Seeds of the homozygous transgenic line containing 35S::VND7-GR were grown in the dark for 3 days at 21 °C on vertical half-strength Murashige and Skoog (MS) plates containing 1% sucrose. Three-day-old *Arabidopsis* seedlings were transferred to microcentrifuge tubes containing liquid half-strength MS medium with 3% sucrose that was supplemented with either 20 µM dexamethasone (DEX) for induced samples or an equivalent volume of the solvent, dimethyl sulfoxide (DMSO), for control seedlings. Seedlings were treated with DEX or DMSO for 60 hours and then collected for SFG analysis.

Celery tracheary elements

Celery tracheary elements were prepared as per the protocol published by D. G. Gray.[42] Vascular bundle strands (approximately 10 to 20 of roughly 10 cm in length) were stripped out of mature petioles and boiled in 1 liter of water for 30 minutes then soaked for 1 hour at room temperature in 1 liter of a 5% w/v NaOH aqueous solution. Strands were then rinsed well and incubated for 1 hour at 35°C in 500 ml of an aqueous solution containing 40 g $NaClO_2$ and 7.5 g CH_3COOH. The bleached white strands were washed several times with a few liters of distilled water until the pH of the wash solution stabilized. The prepared strands were stored moist under refrigeration.

Sum frequency generation spectroscopy

Cellulose crystals are SFG-active because of its noncentrosymmetric space group.[22-23] Thus by temporal and spatial overlapping of two pulsed laser beams, 800 nm and IR, SFG signals can be generated. The 800 nm laser pulse was generated by a Ti-Sapphire amplifier (Coherent, Libra) at 2 kHz repetition rate with 85 fs pulse duration, 12 nm pulse width (full width at half maximum), and 2.4 mJ pulse energy. For improving the spectral resolution, the pulse was narrowed by using two Fabry-Perot etalons to 0.78 nm. The tunable IR was generated with an optical parametric amplifier/generator (OPA/OPG) system (Coherent, OPerA Solo). The broadband IR laser pulses had 150 cm^{-1} – 200 cm^{-1} FWHM, and it can scan from 1000 cm^{-1} to 4000 cm^{-1}. The IR (5 mW – 12 mW) and 800nm (8 mW) laser pulses were directed in parallel to a microscope (Olympus, BX51W1) entrance port and focused on a sample using a 36X reflective objective lens (NA = 0.52, Newport). The incident angle for 800 nm and IR pulses lens was 22.5° ± 7.5° from the opposite sides of the surface normal direction and the irradiated area was about 4.1 μm × 2.4 μm.[33] The broadband SFG signal then passes a monochromator and spectrally

resolves using a volume-phase holographic grating and then collected by a CCD camera. The laser and microscope systems were discussed in details by Lee et al.[43] and Huang et al.[33]

The control experiment with the CNC suspension solution was carried out with a table-top system in a reflection mode.[43] The Arabidopsis and celery experiments were done with the microscopy system in a transmission mode with a 3 μm step scanning. Freshly prepared samples were put in D_2O overnight to replace water (H_2O) in the sample; this allowed probing the OH stretch bands in crystalline cellulose in the sample fully hydrated in D_2O.[16, 33-34] Note that the OH/OD exchange can occur readily at the surface of crystals, but the exchange for core OH groups is an extremely slow process at room temperature because D_2O cannot diffuse into the interior of the crystalline domain.[refs from response letter] The samples were sandwiched between a slide glass and a coverslip and sealed using a nail polish. The SFG signal was collected for CH-CH_2 stretch region (2800 cm^{-1} – 3000 cm^{-1}) and OH stretch region (3200 cm^{-1} – 3500 cm^{-1}) and the hyperspectral imaging processing were done using Mathematica.[33]

Theoretical calculations

The dependence of the SFG intensity of the uniaxially-aligned CMFs on the directionality (unidirectional vs. bidirectional) and the distance between CMFs can be modeled using the non-linear optical theory summing SFG signals from polycrystalline domains with taking into account randomizing phase distribution terms:[44]

$$I_3 \propto I_2 I_1 \left| \sum_{m=1}^{q} \chi_m^{(2)} \frac{e^{-i\Delta k l_m} - 1}{\Delta k} \, e^{-i\Delta k \sum_{j=1}^{m-1} l_j} \right|^2 n^2 \tag{1}$$

$$\chi_m^{(2)} \propto M_{\alpha\beta} A_\gamma \tag{2}$$

$$\Delta k = k_1 + k_2 - k_3 \,, \qquad k_i = \frac{n_i \, \omega_i}{c} \tag{3}$$

$$L_c = \frac{2}{\Delta k} \tag{4}$$

Here I_3, I_2, and I_1 are the intensities of the SFG signal, the 800 nm up-conversion beam, and the resonant IR beam, respectively; $\chi_m^{(2)}$ is an effective second-order susceptibility tensor of the SFG-active vibrational mode of the mth crystal which is the product of Raman ($M_{\alpha\beta}$) and IR (A_γ) transition moments of the crystal at given polarization combinations of SFG, 800 nm, and IR beams; l_m and l_i are the dimension of each domain contributing to the overall SFG; and Δk is the phase mismatch between the SFG signal (k_3) and the sum of the input wave vectors of IR (k_1) and 800 nm (k_2), which can be calculated from the refractive index (n_i) of the medium, the speed of light (c), and the angular frequency (ω_i) of each beam. The magnitude of Δk determines the coherence length (L_c) beyond which the SFG yield becomes insignificant.[37-38] In Eq.(1), the $\frac{e^{-i\Delta k l_m - 1}}{\Delta k}$ term represents the effect of wave vector mismatch on the SFG intensity of the mth domain and the $e^{-i\Delta k \sum_{j=1}^{m-1} l_j}$ term represents the phase randomization effect on the SFG intensity by neighboring domains with different sizes (l_j) or orientations in a polycrystalline medium.[44]

To theoretically explain the difference in SFG intensity dependence on the inter-particle distance (Δl) for the unidirectional and bidirectional CMFs (Figures 2a and 2b), a simplified one-dimensional model system will be considered. In this simplified model (Figure 3), all cellulose crystals are assumed to have the same diameter (d) and the crystal c-axis (chain axis) is aligned along the X-axis in the lab coordinate. The crystals are assumed to have the full 360° rotational degree of freedom along the alignment axis;[45] if there are some degrees of registry between certain crystallographic facets of CMF in cell walls, this assumption can be modified. The tilt angles of the transition dipole moments ($\partial\mu/\partial Q$) of the CH and OH stretch modes are shown in Figure 3 based on the previous theoretical calculations and polarization-IR measurements.[30, 39-40]

For the simplicity of the calculation, the $\chi_m^{(2)}$ orientation will be assumed to be the same as the IR tensor orientation. The previous TD-DFT calculations showed that for the cases of unidirectional and bidirectional packing of crystals, the Raman transition is not significantly different between the two cases;[39] so, it would not affect the model calculation result significantly. The $\chi_m^{(2)}$ term is a positive value when the chain direction is unidirectional and can be positive or negative depending on the directionality along the X-axis when CMFs are bidirectional.

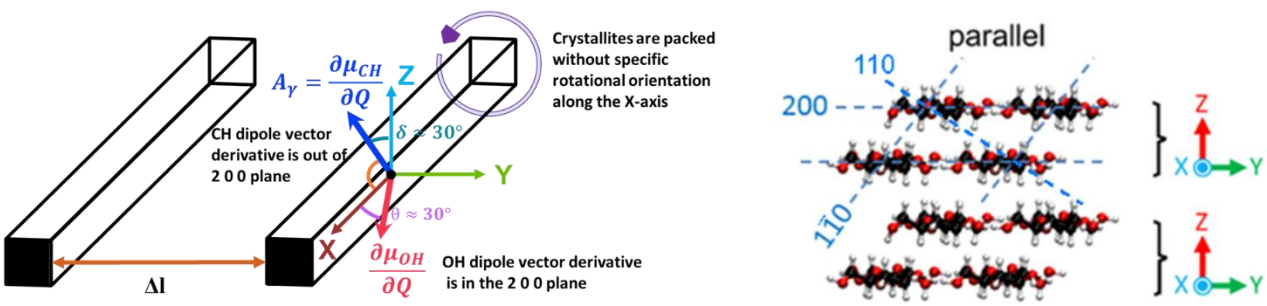

Figure 3. One-dimensional model for the theoretical calculation of the SFG intensity as a function of the interparticle separation distance (Δl). The image in the right shows eight chains of cellulose in the Iβ allomorph along the chain axis. When the (200) plane of cellulose Iβ is in the XY plane of the lab coordinate and the c-axis is aligned to the X-axis, the transition dipole moment of the CH stretch mode is assumed to be tilted by 60° from the X-axis toward the Z-axis (away from the (200) plane; thus, δ ≈ 30°). The transition dipole moment of the OH stretch mode is tilted by 30° from the chain axis toward the Y-axis (within the (200) plane). These angles are chosen for the simulation based on the TD-DFT calculations and the polarization IR measurements.30, 39-40 The right image is copied from Ref. 39 with permission conveyed from Copyright Clearance Center Inc.

In this model, the domain size (l_m) can be assumed to be either the diameter of the cellulose crystal (d) or the distance between the crystals (Δl) and these two domains appear alternatively along the Y-direction in Figure 3. Thus, in Eq.(1), odd m's are cellulose crystals ($\chi_{odd}^{(2)} \neq 0$; ± depending on the chain directionality along the X-axis) and even m's are amorphous domains ($\chi_{even}^{(2)} = 0$). It also simplifies the summation term of the exponent in the

phase randomization factor to $\sum_{j=1}^{m-1} l_j = \left\lceil \frac{m-1}{2} \right\rceil d + \left\lfloor \frac{m-1}{2} \right\rfloor \Delta l$. Then, Eq.(1) for the unidirectional and bidirectional packing of cellulose crystals can be converted to Eq.(5) and Eq.(6), respectively:

$$I_3 \propto \left| \sum_{f=1}^{n-1} I_2 I_1 e^{-f(d+\Delta l)} \chi_1^{(2)} d^{\cancel{2}} \frac{e^{-i\Delta k d} - 1}{\Delta k} \left(e^{-i\Delta k (d+\Delta l) f}\right) (\cos\theta + \cos\delta \sin\theta) \right|^2 n^2 \quad (5)$$

$$I_3 \propto \left| \sum_{f=1}^{n-1} I_2 I_1 e^{-f(d+\Delta l)} \chi_1^{(2)} d^{\cancel{2}} \frac{e^{-i\Delta k d} - 1}{\Delta k} \left(e^{-i\Delta k (d+\Delta l) f}\right) ((-1)^f (\cos\theta) + \cos\delta \sin\theta) \right|^2 n^2 \quad (6)$$

where θ is the polar angle of the transition dipole vector from the X axis, δ is the tilt angle between the transition dipole vector from the Z-axis, and n is the number of crystals within the coherence length along the Y-direction, $n = L_c/(d + \Delta l)$.

Note that Eq.(5) and Eq.(6) are the simplified versions of Eq.(1) showcasing the hypothetical condition of the perfectly-unidirectional and alternatively-bidirectional packings of the uniaxially-aligned crystals of the same size with the identical separation distance in one dimension. These equations do not replicate the exact situation of CMFs in plant cell walls which are deviating from the ideal case shown in Figure 3. However, the solutions of these equations can provide physical insights needed to determine the CMF directionality from the SFG spectra of plant cell walls. The full Mathematica program solving these equations numerically with the random distribution of crystal orientation around the X-axis is provided in the Supporting Information.

It should be noted that the physical system considered here is different from the phase-sensitive SFG or second harmonic generation (SHG) used to determine the average or net polarity of molecules at two dimensional (2D) interfaces. In the phase-sensitive detection method, the signals from the interfacial molecules (which are all within the coherence length) are

mixed with an externally-generated reference signal with a known phase at the same frequency of SFG or SHG signal; then, the net polarity (i.e., "pointing-up" vs. "pointing-down") of molecules with respect to the 2D plane is determined.[46-49] This existing phase-sensitive detection method would be difficult to apply to crystalline cellulose interspersed three-dimensionally in an amorphous matrix because the SFG signal comes from the entire probe volume that is often larger than the coherence length dimension. A digital holographic imaging could extract the intensity and phase information over an extended depth of focus;[50] but, it requires scanning one wavelength at a time and has not been demonstrated for the broadband SFG. Based on the theoretical model discussed here, one can determine the "relative phase" of SFG-active domains within the coherence length if there are two peaks that have different symmetry cancellation efficiency. In the case of CMFs, the symmetry cancellation effects of the CH and OH signal are found to be different upon parallel (unidirectional) vs. antiparallel (bidirectional) packing.[39, 51] The theoretical consideration presented here cannot determine the "absolute phase" of CMFs with respect to the lab frame because the external reference beam is not used.

Results & Discussion

Theoretical prediction for unidirectional vs. bidirectional packing in one dimension

Figure 4a plots the SFG intensities calculated for the CH and OH stretch modes of uniaxially-aligned cellulose crystals with d = 5 nm as a function of Δl for the unidirectional (Eq.(5)) and bidirectional (Eq.(6)) packing. This crystal diameter is chosen because the CMFs in plant cell walls are typically 3-5 nm in diameter.[52] A case with d = 20 nm is shown in the

Supporting Information for comparison. In this calculation, the SFG coherence (L_c) is set as 120 nm, which is the value calculated for our experimental reflection geometry.[41, 43]

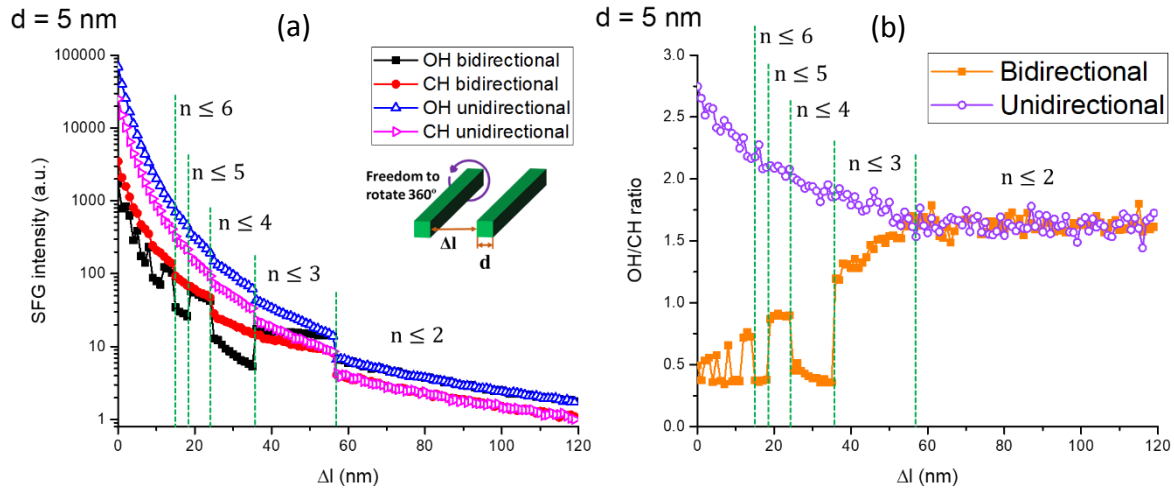

Figure 4. (a) Theoretical prediction of the CH and OH stretch modes for the unidirectional (open symbols) and bidirectional (filled symbols) packing of cellulose crystals (modeled in Figure 3) as a function of Δl. Here, n indicates the number of crystals within the SFG coherence length (L_c) and the diameter of each crystal (d) is 5 nm. (b) Theoretically calculated OH/CH intensity ratio for the unidirectional and bidirectional uniaxial packing of cellulose crystals as a function of Δl. Each data point is the average of calculation results for 1000 orientations of the (200) plane created with a random function generator.

For the unidirectional packing case, both CH and OH SFG intensities increase monotonically as Δl decreases, which is the consequence of the increase in the cellulose concentration within L_c. In our simple one-dimensional model, n increases in integer; so, there is a sudden jump whenever n changes. This is just an artifact of the simplified one-dimensional model. In reality, the SFG intensity will vary smoothly as the cellulose concentration increases in the sample, because of local variances in inter-CMF distances and CMF angles.

In the case of bidirectional packing, the OH SFG intensity increases as Δl decreases within the same n range but significantly drops when n varies from odd numbers to even numbers (for example, n≤3 → n≤4). This is because the symmetry cancellation effect of the OH transition dipoles pointing toward the opposite directions is larger than the concentration increase

effect (n^2 in Eq.(6)) at that specific Δl region. In contrast, the symmetry cancellation effect is relatively insignificant for the CH transition dipoles; thus, the SFG intensity drop is negligible at the change of n from odd numbers to even numbers.

Figure 4b compares the ratio of the calculated SFG intensities of the OH and CH stretch modes for the uniaxially aligned cellulose crystals with the unidirectional versus bidirectional packing. In the unidirectional packing, the OH/CH ratio increases monotonically from the fully isolated case ($\Delta l \geq L_c$) to the intimate contact case (Δl = 0). In contrast, the OH/CH ratio of the bidirectional packing decreases from the fully isolated case in a non-monotonic and sinusoidal way with a decreasing periodicity as Δl decreases from L_c to zero.

The calculation result for the simple one-dimensional model suggests that if one can estimate the inter-CMF distance (Δl) from the volumetric concentration of cellulose in the sample and knows that CMFs are aligned uniaxially along the main MFA axis form x-ray diffraction,[4, 17] then the average directionality of the CMFs in the sample can be determined by measuring the OH/CH intensity ratio of cellulose in SFG (Figure 4b). Note that the theoretical calculation predicting the SFG OH/CH intensity ratio of CMFs in the real sample is extremely difficult and much more complicated because the angle and separation distance of CMFs vary locally within the sample.[12, 53-54]

The data in Figure 4a also suggest that the CH SFG intensities of different samples (for example, at different growth stages) can be used to compare the relative concentration of CMFs in the samples as long as the CMF packing pattern and directionality do not change between samples.[55-56] But, the OH SFG intensity cannot be used for such purposes when CMFs are packed bidirectionally.[51] The quantitative comparison of the absolute intensity in experimental data with the calculation result is not possible because of complications from local structural

variations and scattering of the light in opaque plant cell walls. However, these complications do not matter in the case of the directionality study since the CH SFG intensity is used as an internal standard to normalize the OH SFG intensity (Figure 4b).

Verification of theoretical prediction for uniaxial packing without preferential directionality

There are many ways to prepare the uniaxially-aligned CNC samples; such methods include mechanical stretching of a polymer matrix in which CNCs are interspersed,[51] shear-assisted deposition of CNCs into thin films,[22] and suspension of CNCs in a capillary tube filled with water with extremely low ionic strength. In all these methods, it is thermodynamically difficult (if not impossible) to align CNCs with the unidirectional polarity. The random directionality along the alignment axis is entropically favorable, which is equivalent to the bidirectional packing in average over the space. Among these methods, we chose the CNC suspension method because small angle x-ray diffraction (SAXS) analysis showed that the CNCs suspended in pure water form a hexagonally packed array with a constant inter-particle distance.[57] Due to the viscosity increase at high CNC concentrations, the practical upper limit of the CNC concentration was ~4 wt.% to use the capillary method. Using a simple geometry argument, the inter-particle distance (Δl) is calculated to be ~58 nm at 4 wt.% (see the Supporting Information). By diluting this solution, a series of uniaxially-aligned CNCs with the bidirectional packing and varying Δl could be prepared.

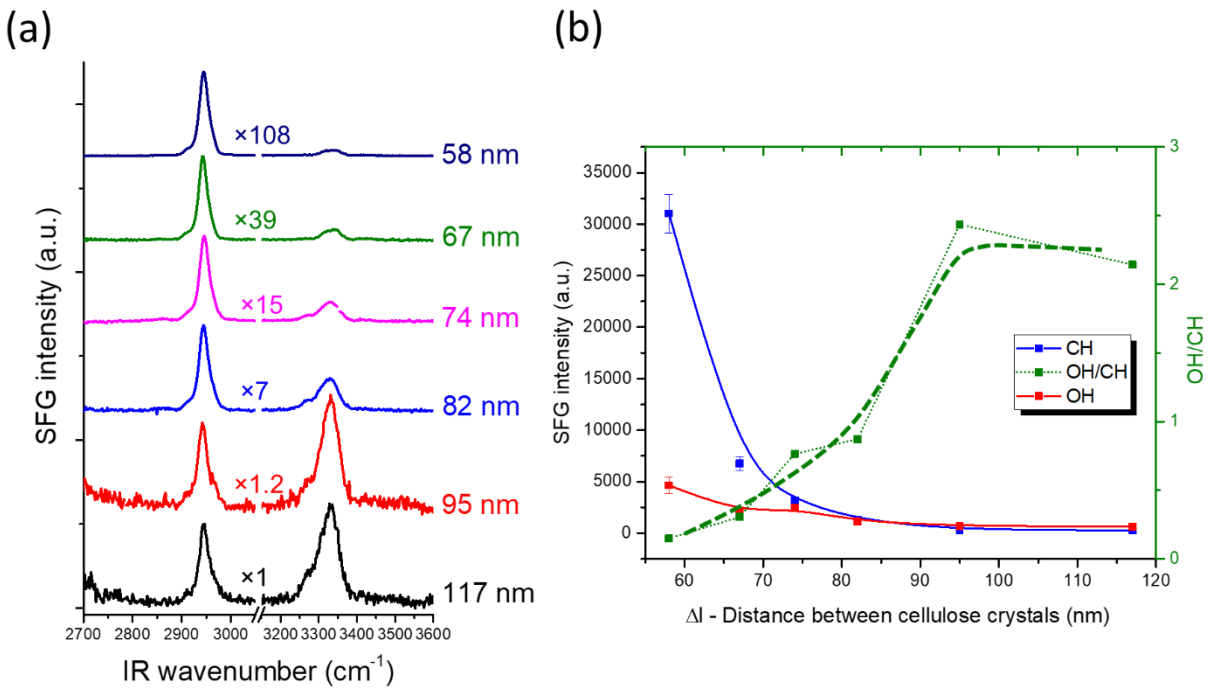

Figure 5. (a) SFG spectra of uniaxially-aligned CNCs dispersed in D_2O in a rectangular capillary tube. The alignment direction is along the capillary tube.[58] The SFG spectra were collected in the reflection geometry with the *ssp* polarization; the number next to each spectrum is the relative intensity of the CH peak used for normalization of the spectrum for comparison. The inter-particle distance was calculated from the CNC concentration (see the Supporting Information). The directionality of CNCs in the suspension is random along the alignment axis, thus it is equivalent to the bidirectional packing in average over the coherence length scale. (b) Plots of CH and OH SFG areas (in the left y-scale) and the OH/CH ratio (in the right y-axis) Cellulose crystals extracted from tunicate were dispersed in D_2O, where they form hexagonal arrays all aligned along the capillary tube.

The SFG spectra of the uniaxially-aligned and bidirectional CNCs with inter-particle distances (Δl) varying from ~58 nm to ~117 nm are shown in Figure 5a. In the reflection-SFG geometry used in this experiment, the coherence length (L_c) is calculated to be ~120 nm (Supporting Information – Mathematica code). The OH and CH SFG peak areas as well as their ratios are plotted in Figure 5b. As predicted in Figure 4a for the bidirectional packing, both OH and CH intensities increase as Δl decreases, but the CH intensity becomes larger than the OH intensity at short Δl distances. Since $L_c \approx 120$ nm, the OH/CH ratio at $\Delta l \approx 117$ nm can be

assumed to be the ratio of intrinsic $\chi_{OH}^{(2)}$ and $\chi_{CH}^{(2)}$ values without inter-particle interferences. When $\Delta l > L_c$, the intensity of SFG is not influenced by the dipole cancellation. Thus, the relative SFG intensities can be directly related to the relative magnitudes of the second-order susceptibility tensors (Eq.(2)) of the OH and CH stretch modes. As Δl decreases below L_c, the OH/CH ratio decreases as predicted in Figure 4b for the bidirectional packing. Although the sinusoidal variance (Figure 5b) is not as clear as the prediction from the simple one-dimensional model (Figure 4a), the experimentally-observed trend is qualitatively consistent with the symmetry cancellation effect considered in the theoretical calculation for the uniaxial packing with the bidirectional packing.

Evidence for the unidirectional packing of CMFs in SCW of transdifferentiated xylem cells

In the previous volume-averaged SFG analysis of SCWs of land plants, the OH SFG intensity of cellulose was found to be much smaller than the CH SFG intensity.[41] This was interpreted that the majority of CMFs in the land plants with thickened SCWs are effectively bidirectional to each other. However, live-cell imaging of fluorescent protein-tagged CSCs during the SCW formation in transdifferentiated xylem cells suggested that the CSC movements are not bidirectional with the equal probability of moving towards the opposite directions along the microtubule.[12] If so, the CMFs in those cell walls will not be fully bidirectional; they will have some degree of unidirectionality. Thus, this system was chosen for the directionality study with SFG.

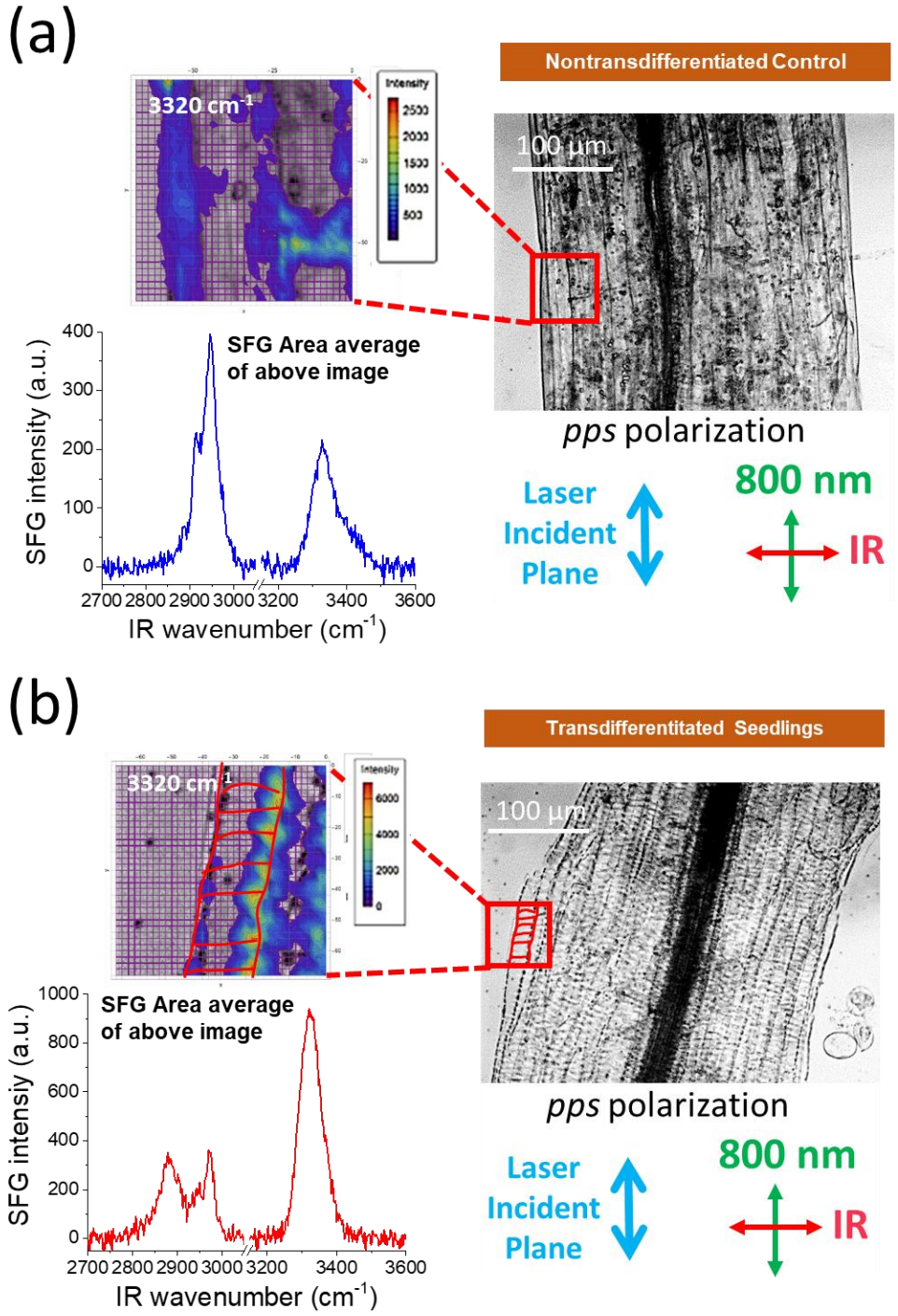

(200

Figure 6. Microscopic SFG analysis of (a) nontransdifferentiated and (b) transdifferentiated epidermis of *Arabidopsis* hypocotyl never-dried and fully-hydrated in D_2O. The optical image of each sample is shown with the scale bar (100 µm). An area of 70 µm × 70 µm (marked with a box) was analyzed with a 2 µm step interval. The broadband SFG spectra were collected in the CH and OH regions at each image pixel; the SFG intensity at 3320 cm^{-1} is shown in the 2D map. The full spectra of the CH and OH regions shown here are constructed by taking the area-average of the raw SFG data from each pixel.

Figure 6 shows the SFG analysis results for nontransdifferentiated and transdifferentiated cells of the *Arabidopsis* hypocotyl. The hoop-shaped cell walls can be recognized in Figure 6b, indicating that the DEX treatment successfully induced transdifferentiation of epidermal cells of *Arabidopsis* hypocotyls into xylem vessel elements.[12] The SFG mapping of 3320 cm^{-1} peak shows stronger intensities near the cell boundaries because a larger amount of cell wall was projected to the image plane at that location. The cellulose-containing wall exists only at the external surface of each cell which is larger than the SFG probe depth of this experiment. Our SFG microscope system has an effective probe depth (depth of focus) larger than 10 μm. Thus, the vertical regions of the cell wall at the cell boundaries fills a larger fraction of the probe volume than the horizontal walls in the top and bottom regions of the cell. In the area-averaged SFG spectrum of the nontransdifferentiated control, the CH peak at 2944 cm^{-1} is stronger than the OH peak at 3320 cm^{-1} (Figure 6a). In contrast, the SCWs in transdifferentiated xylem cells show the OH SFG intensity much stronger than the CH SFG intensity (Figure 6b) (also, see Figure S2). This high OH/CH SFG intensity ratio supports that the CMFs in SCWs of transdifferentiated xylem cells are not entirely bidirectional; they must have some degree of unidirectionality, which is congruent with the biased unidirectionality found in the CSC movement tracking for the same sample.[12]

It is reasonable to expect that the cellulose content is higher in transdifferentiated xylem cells than that in nontransdifferentiated control; however, this cannot be responsible for the OH/CH intensity ratio difference between the control and transdifferentiated xylem cells. If the CMFs were effectively bidirectional in SCWs of transdifferentiated cells, then the OH/CH intensity ratio would have been lower than the nontransdifferentiated cells because of the larger

symmetry cancellation effect for the higher cellulose concentration sample (thus, smaller Δl in Figures 4b and 5b). That is the opposite to the experimental observation. Thus, the high OH/CH SFG intensity ratio must be due to the "net" unidirectional packing of CMFs in the transdifferentiated xylem cells.

It is important to note that the OH/CH ratio in biological tissues can vary by multiple factors. The change in the orientation of microfibrils can impact the OH/CH ratio as the microfibril relative position with respect to the laser incidence plane can vary depending on the analyzed location. The bundling of microfibrils can also affect the OH/CH ratio. The OH/CH ratios can also be affected by the existence of non-cellulosic compounds in the probing area which can absorb the IR beam in one region (CH or OH) more than the other. The investigation on all these possibilities is beyond the scope of this study.

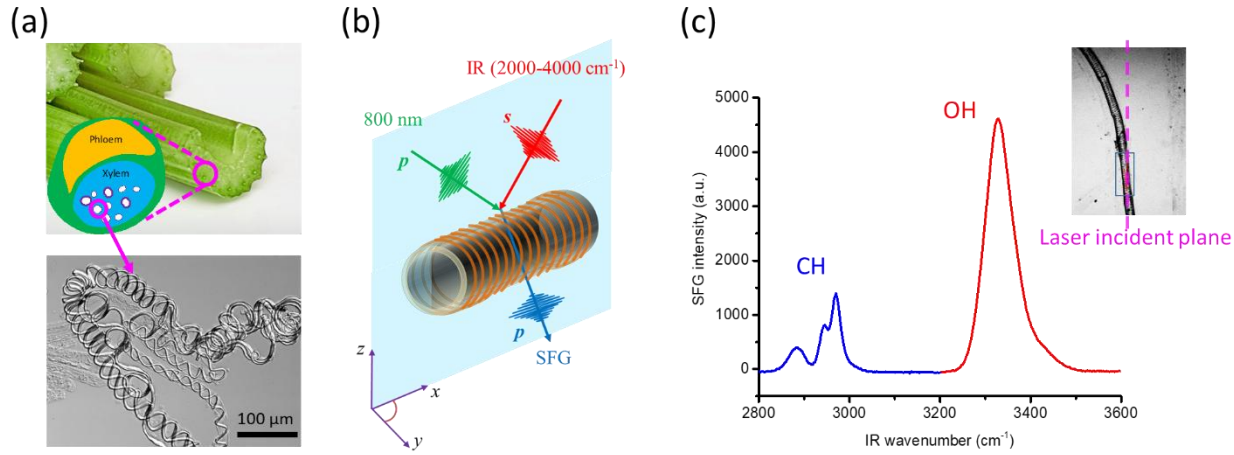

Figure 7. (a) Optical image of celery cross-section and the microscopic image of cellulose macrofibril coils isolated from the tracheary elements. (b) Experimental geometry of the transmission-SFG measurement. The coil axis is placed in the laser incidence plane and the SFG polarization combination is *pps*; thus, the IR polarization is nearly parallel to individual cellulose microfibrils. (c) SFG spectrum of the cellulose macrofibril coil aligned along the laser incidence plane. The SFG spectrum of the coil aligned perpendicular to the laser incidence plane is shown in Figure S3.

Cellulose coils in tracheary elements of celery can be isolated,[42] which make them an ideal sample for SFG analysis of the CMF directionality (polar ordering) without contributions of SFG signals from other types of cell walls. Figure 7a shows the optical microscope image of the cellulose macrofibrils isolated from celery treachery coils. Their diameter is about 2-3 μm. The sugar analysis of the celery treachery element indicated that the cellulose content is ~75%,[42] which would correspond to an inter-CMF distance of ~4 nm (side to side) assuming the full dispersion of individual 4 nm thick CMFs in the sample. Using the transmission geometry of the SFG measurement sketched in Figure 7b, the coherence length is estimated to be ~6.3 μm; thus, $\Delta l/L_c \approx 0.0003$. This sample gives the OH/CH intensity ratio of ~5, which is significantly larger than the intrinsic $\chi_{OH}^{(2)}/\chi_{CH}^{(2)}$ ratio (~2.3 in Figure 5b) of cellulose Iβ estimated from the $\Delta l \approx L_c$ case. In the one-dimensional model calculation for the unidirectional packing (Figure 4b), the OH/CH intensity ratio is predicted to increase almost by a factor of 2 as $\Delta l/L_c$ approaches zero, compared to the $\Delta l/L_c$ = 1 case. The preferential orientation of the CMFs with respect to the laser incidence plane cannot explain this large OH/CH ratio (Figure S3). The comparison of the experimental value (Figures 6c and S3) with this theoretical prediction (Figure 4b) suggests that the elementary CMFs in the celery tracheary element coil must have a high degree of unidirectional polarity.

One may question if the chirality of cellulose may influence the OH/CH intensity ratio upon switching the directionality from the parallel (unidirectionally biased) to antiparallel (bidirectional) packing. The SFG of cellulose does not follow the conventional achiral/chiral rule of the SFG of the 2D surface with the C_∞ symmetry. Figure S4 compares the SFG spectra collected with different polarization combinations known to be sensitive to chiral and achiral molecules for a reference sample created by uniaxial packing of cellulose Iβ crystals isolated

from tunicate. Since the uniaxial packing was induced during the solution evaporation with a shear force,[22] there is no preferential directionality of the cellulose crystals along the preferential packing axis. In Figure S4, the *ppp*-SFG spectrum of cellulose crystals aligned along the laser incidence plane is almost identical to the *sss*-SFG spectrum of cellulose aligned perpendicular to the laser incidence plane. Similarly, the *pps* spectrum for the in-plane orientation is very similar to the *ssp* spectrum of the out-of-plane orientation, and so on. This means that the SFG spectral features of cellulose are more sensitive to the azimuth angle dependence than the chiral/achiral polarization combination. Still the azimuth angle dependence alone (Figure S4) cannot explain the OH/CH intensity ratio larger than 2 for the uniaxially-aligned CMFs.

The data shown in Figures 6 and 7 imply that CMFs in xylem or xylem-like cells in other plants may have the unidirectional packing. This is in stark contrast to the fully-developed cotton fibers which give the OH/CH ratio of ~0.2,[56] indicating almost perfect bidirectional packing. These experimental observations raise a few important questions that have not been asked or systematically studied in plant biology. What controls the directionality (or polarity) of the CSC movement during the cellulose synthesis? How is the CMF directionality associated with the biological and mechanical functions of the cell at the specific growth stage of the plant? The theoretical foundation and experimental confirmation reported in this paper open an unprecedented opportunity to study these questions related to the cellulose biosynthesis with SFG. The same principle and methodology can also be applied to other crystalline biopolymers such as chitin, amylose, collagen, etc. that are SFG-active due to their non-centrosymmetric crystal structures.[59-61]

Conclusions

In this study, theoretical calculations were combined with experiments to prove the sensitivity of SFG to the nano-/meso-scale arrangement of cellulose crystals in amorphous matrices. The transition dipole moments of cellulose and the phase synchronization principle of SFG were incorporated in the theoretical calculation for a simplified one-dimensional model to study the effect of crystal polarity and intercrystallite distance on the SFG intensity. From the calculations, the ratio of SFG peaks in OH and CH stretch regions (OH/CH) was found to be highly dependent on the polar order (unidirectional vs. bidirectional) of uniaxially-aligned cellulose crystals and the distance between the crystals. The OH/CH ratio increases for the unidirectional-packing case and decreases for the bidirectional-packing case as the distance between crystals decreases. As the inter-crystal distance increases to the SFG coherence length, the OH/CH ratios of both cases converge to the intrinsic value of isolated crystals without spectral interferences to each other. The theoretical prediction for the bidirectional packing of cellulose crystals was confirmed experimentally. Based on the theoretically predicted and experimentally proven trends, it was found for the first time that the induced xylem cells of Arabidopsis and celery tracheary elements have the biased unidirectional packing of cellulose microfibrils in the cell wall.

Acknowledgements. The theoretical calculations and verification with uniaxially-aligned CNC suspensions were conducted with the support by the Center for Lignocellulose Structure and Formation, Energy Frontier Research Center funded by the U.S. Department of Energy, Office of Science, Basic Energy Sciences, under Award Number DE-SC0001090. The study on the transdifferentiated xylem cells of Arabidopsis and tracheary cellulose coils of celery was carried

out as a part of iSuperSEED program of the Penn State MRSEC funded by the National Science Foundation (Grant no. DMR-1420620).

Supporting Information: Calculation of distance between crystals with a hexagonal lateral packing. The SFG intensity calculations for CH and OH stretch modes for 20 nm width crystals as a function of intercrystallite distance. The control experiments for xylem induced hypocotyls. The SFG analysis for rotation of celery coils by 90° with respect to laser incident plane. Polarization dependence of SFG signal for uniaxially aligned cellulose crystals. The Mathematica code to calculate the SFG intensity of CH and OH stretch modes for unidirectional and bidirectional packing of crystals.

References

1. Albersheim, P.; Darvill, A.; Roberts, K.; Sederoff, R.; Staehelin, A., *Plant cell walls*. Garland Science, Taylor & Francise Group: New York, 2010.
2. Cosgrove, D. J., Growth of the plant cell wall. *Nat. Rev. Mol. Cell. Biol.* **2005,** *6* (11), 850-61.
3. Bergfeld, R.; Speth, V.; Schopfer, P., Reorientation of Microfibrils and Microtubules at the Outer Epidermal Wall of Maize Coleoptiles During Auxin-Mediated Growth. *Botanica Acta* **1988,** *101* (1), 57-67.
4. Reiterer, A.; Lichtenegger, H.; Tschegg, S.; Fratzl, P., Experimental evidence for a mechanical function of the cellulose microfibril angle in wood cell walls. *Philos. Mag. A* **1999,** *79* (9), 2173-2184.
5. Zhong, R.; Burk, D. H.; Morrison, W. H.; Ye, Z.-H., A Kinesin-Like Protein Is Essential for Oriented Deposition of Cellulose Microfibrils and Cell Wall Strength. *Plant Cell* **2002,** *14* (12), 3101.
6. Burk, D. H.; Ye, Z.-H., Alteration of Oriented Deposition of Cellulose Microfibrils by Mutation of a Katanin-Like Microtubule-Severing Protein. *Plant Cell* **2002,** *14* (9), 2145.
7. Arantes, V.; Saddler, J. N., Access to cellulose limits the efficiency of enzymatic hydrolysis: the role of amorphogenesis. *Biotechnol. Biofuels* **2010,** *3* (1), 4.
8. Chundawat, S. P. S.; Beckham, G. T.; Himmel, M. E.; Dale, B. E., Deconstruction of Lignocellulosic Biomass to Fuels and Chemicals. *Annu. Rev. Chem. Biomol. Eng.* **2011,** *2* (1), 121-145.

9. Zhang, Y. H. P., Reviving the carbohydrate economy via multi-product lignocellulose biorefineries. *J. Ind. Microbiol. Biotechnol.* **2008,** *35* (5), 367-375.
10. Donaldson, L., Cellulose microfibril aggregates and their size variation with cell wall type. *Wood Sci. Technol.* **2007,** *41* (5), 443.
11. Anderson, C. T.; Carroll, A.; Akhmetova, L.; Somerville, C., Real-time imaging of cellulose reorientation during cell wall expansion in Arabidopsis roots. *Plant physiol.* **2010,** *152* (2), 787-796.
12. Li, S.; Bashline, L.; Zheng, Y.; Xin, X.; Huang, S.; Kong, Z.; Kim, S. H.; Cosgrove, D. J.; Gu, Y., Cellulose synthase complexes act in a concerted fashion to synthesize highly aggregated cellulose in secondary cell walls of plants. *Proc. Natl. Acad. Sci. U. S. A.* **2016,** *40*, 11348–1135.
13. Zheng, Y.; Cosgrove, D. J.; Ning, G., High-resolution field emission scanning electron microscopy (FESEM) imaging of cellulose microfibril organization in plant primary cell walls. *Microsc. Microanal.* **2017,** *23* (5), 1048-1054.
14. Xu, P.; Donaldson, L. A.; Gergely, Z. R.; Staehelin, L. A., Dual-axis electron tomography: a new approach for investigating the spatial organization of wood cellulose microfibrils. *Wood Sci. Techol.* **2006,** *41* (2), 101.
15. Reza, M.; Ruokolainen, J.; Vuorinen, T., Out-of-plane orientation of cellulose elementary fibrils on spruce tracheid wall based on imaging with high-resolution transmission electron microscopy. *Planta* **2014,** *240* (3), 565-573.
16. Huang, S.; Kiemle, S. N.; Makarem, M.; Kim, S. H., Correlation between crystalline cellulose structure and cellulose synthase complex shape: a spectroscopic study with unicellular freshwater alga Micrasterias. *Cellulose* **2020,** *27* (1), 57-69.
17. Barnett, J. R.; Bonham, V. A., Cellulose microfibril angle in the cell wall of wood fibres. *Biol. Rev.* **2004,** *79* (2), 461-472.
18. Giddings, T. H., Jr.; Brower, D. L.; Staehelin, L. A., Visualization of particle complexes in the plasma membrane of Micrasterias denticulata associated with the formation of cellulose fibrils in primary and secondary cell walls. *J. Cell. Biol.* **1980,** *84* (2), 327-339.
19. Newman, R. H.; Hill, S. J.; Harris, P. J., Wide-angle x-ray scattering and solid-state nuclear magnetic resonance data combined to test models for cellulose microfibrils in mung bean cell walls. *Plant Physiol.* **2013,** *163* (4), 1558-1567.
20. Saxe, F.; Eder, M.; Benecke, G.; Aichmayer, B.; Fratzl, P.; Burgert, I.; Rüggeberg, M., Measuring the distribution of cellulose microfibril angles in primary cell walls by small angle X-ray scattering. *Plant Methods* **2014,** *10* (1), 25.
21. Ye, D.; Kiemle, S. N.; Rongpipi, S.; Wang, X.; Wang, C.; Cosgrove, D. J.; Gomez, E. W.; Gomez, E. D., Resonant soft X-ray scattering reveals cellulose microfibril spacing in plant primary cell walls. *Sci. Rep.* **2018,** *8* (1), 12449.
22. Nishiyama, Y.; Langan, P.; Chanzy, H., Crystal structure and hydrogen-bonding system in cellulose Iβ from synchrotron X-ray and neutron fiber diffraction. *J. Am. Chem. Soc.* **2002,** *124* (31), 9074-9082.
23. Nishiyama, Y.; Sugiyama, J.; Chanzy, H.; Langan, P., Crystal structure and hydrogen bonding system in cellulose Iα from synchrotron X-ray and neutron fiber diffraction. *J. Am. Chem. Soc.* **2003,** *125* (47), 14300-14306.

24. Atalla, R. H.; Vanderhart, D. L., Studies on the structure of cellulose using Raman spectroscopy and solid state C NMR. In *Cellulose and wood-chemistry and technology*, Wiley: New York, 1988; pp 169–188.
25. Horii, F.; Hirai, A.; Kitamaru, R., Solid-state 13 C-NMR study of conformations of oligosaccharides and cellulose. *Polym. Bull.* **1983,** *10* (7-8), 357-361.
26. Wang, T.; Hong, M., Solid-state NMR investigations of cellulose structure and interactions with matrix polysaccharides in plant primary cell walls. *J. Exp. Bot.* **2015,** *67* (2), 503-514.
27. Wang, T.; Park, Y. B.; Daniel, J. C.; Hong, M., Cellulose-pectin spatial contacts are inherent to never-dried Arabidopsis thaliana primary cell walls: evidence from solid-state NMR. *Plant physiol.* **2015,** *168*, 871-884.
28. Blackwell, J., Infrared and Raman spectroscopy of cellulose. In *Cellulose Chemistry and Technology*, American Chemical Society: 1977; Vol. 48, pp 206-218.
29. Cael, J.; Gardner, K.; Koenig, J.; Blackwell, J., Infrared and Raman spectroscopy of carbohydrates. Paper V. Normal coordinate analysis of cellulose I. *J. Chem. Phys.* **1975,** *62* (3), 1145-1153.
30. Makarem, M.; Lee, C. M.; Kafle, K.; Huang, S.; Chae, I.; Yang, H.; Kubicki, J. D.; Kim, S. H., Probing cellulose structures with vibrational spectroscopy. *Cellulose* **2019,** *26* (1), 35-79.
31. Xu, F.; Yu, J.; Tesso, T.; Dowell, F.; Wang, D., Qualitative and quantitative analysis of lignocellulosic biomass using infrared techniques: A mini-review. *Appl. Energy* **2013,** *104*, 801-809.
32. Barnette, A. L.; Bradley, L. C.; Veres, B. D.; Schreiner, E. P.; Park, Y. B.; Park, J.; Park, S.; Kim, S. H., Selective detection of crystalline cellulose in plant cell walls with sum-frequency-generation (SFG) vibration spectroscopy. *Biomacromolecules* **2011,** *12* (7), 2434-9.
33. Huang, S.; Makarem, M.; Kiemle, S. N.; Hamedi, H.; Sau, M.; Cosgrove, D. J.; Kim, S. H., Inhomogeneity of Cellulose Microfibril Assembly in Plant Cell Walls Revealed with Sum Frequency Generation Microscopy. *J. Phys. Chem. B* **2018,** *122* (19), 5006-5019.
34. Huang, S.; Makarem, M.; Kiemle, S. N.; Zheng, Y.; He, X.; Ye, D.; Gomez, E. W.; Gomez, E. D.; Cosgrove, D. J.; Kim, S. H., Dehydration-induced physical strains of cellulose microfibrils in plant cell walls. *Carbohydr. polym.* **2018,** *197*, 337-348.
35. Lambert, A. G.; Davies, P. B.; Neivandt, D. J., Implementing the Theory of Sum Frequency Generation Vibrational Spectroscopy: A Tutorial Review. *Appl. Spectrosc. Rev.* **2005,** *40* (2), 103-145.
36. Wang, H. F.; Gan, W.; Lu, R.; Rao, Y.; Wu, B. H., Quantitative spectral and orientational analysis in surface sum frequency generation vibrational spectroscopy (SFG-VS). *Int. Rev. Phys. Chem.* **2005,** *24* (2), 191-256.
37. Boyd, R. W.; Boyd, R. W., *Nonlinear Optics*. Elsevier Science: Burlington, UNITED STATES, 2003.
38. Shen, Y.-R., The principles of nonlinear optics. *New York, Wiley-Interscience, 1984, 575 p.* **1984**.
39. Lee, C. M.; Chen, X.; Weiss, P. A.; Jensen, L.; Kim, S. H., Quantum Mechanical Calculations of Vibrational Sum-Frequency-Generation (SFG) Spectra of Cellulose: Dependence of the CH and OH Peak Intensity on the Polarity of Cellulose Chains within the SFG Coherence Domain. *J. Phys. Chem. Lett.* **2017,** *8* (1), 55-60.

40. Lee, C. M.; Kubicki, J. D.; Fan, B.; Zhong, L.; Jarvis, M. C.; Kim, S. H., Hydrogen-bonding network and OH stretch vibration of cellulose: Comparison of computational modeling with polarized IR and SFG spectra. *J. Phys. Chem. B* **2015,** *119* (49), 15138-49.
41. Lee, C. M.; Kafle, K.; Park, Y. B.; Kim, S. H., Probing crystal structure and mesoscale assembly of cellulose microfibrils in plant cell walls, tunicate tests, and bacterial films using vibrational sum frequency generation (SFG) spectroscopy. *Phys. Chem. Chem. Phys.* **2014,** *16* (22), 10844-53.
42. Gray, D. G., Isolation and handedness of helical coiled cellulosic thickenings from plant petiole tracheary elements. *Cellulose* **2014,** *21* (5), 3181-3191.
43. Lee, C. M.; Kafle, K.; Huang, S.; Kim, S. H., Multimodal broadband vibrational sum frequency generation (MM-BB-V-SFG) spectrometer and microscope. *J. Phys. Chem. B* **2016,** *120* (1), 102-16.
44. Baudrier-Raybaut, M.; Haïdar, R.; Kupecek, P.; Lemasson, P.; Rosencher, E., Random quasi-phase-matching in bulk polycrystalline isotropic nonlinear materials. *Nature* **2004,** *432*, 374.
45. Terrett, O. M.; Lyczakowski, J. J.; Yu, L.; Iuga, D.; Franks, W. T.; Brown, S. P.; Dupree, R.; Dupree, P., Molecular architecture of softwood revealed by solid-state NMR. *Nat. Commun.* **2019,** *10* (1), 4978.
46. Rivard, M.; Popov, K.; Couture, C.-A.; Laliberté, M.; Bertrand-Grenier, A.; Martin, F.; Pépin, H.; Pfeffer, C. P.; Brown, C.; Ramunno, L.; Légaré, F., Imaging the noncentrosymmetric structural organization of tendon with Interferometric Second Harmonic Generation microscopy. *J. Biophotonics* **2014,** *7* (8), 638-646.
47. Rivard, M.; Couture, C.-A.; Miri, A. K.; Laliberté, M.; Bertrand-Grenier, A.; Mongeau, L.; Légaré, F., Imaging the bipolarity of myosin filaments with Interferometric Second Harmonic Generation microscopy. *Biomed. Opt. Express* **2013,** *4* (10), 2078-2086.
48. Han, Y.; Raghunathan, V.; Feng, R.-r.; Maekawa, H.; Chung, C.-Y.; Feng, Y.; Potma, E. O.; Ge, N.-H., Mapping Molecular Orientation with Phase Sensitive Vibrationally Resonant Sum-Frequency Generation Microscopy. *J. Phys. Chem. B* **2013,** *117* (20), 6149-6156.
49. Sun, S.; Bisson, P. J.; Bonn, M.; Shultz, M. J.; Backus, E. H. G., Phase-Sensitive Sum-Frequency Generation Measurements Using a Femtosecond Nonlinear Interferometer. *J. Phys. Chem. C* **2019,** *123* (12), 7266-7270.
50. Ma, D.; Lee, C. M.; Chen, Y.; Mehta, N.; Kim, S. H.; Liu, Z., Vibrational sum frequency generation digital holography. *Appl. Phys. Lett.* **2017,** *110* (25), 251601.
51. Makarem, M.; Sawada, D.; O'Neill, H. M.; Lee, C. M.; Kafle, K.; Park, Y. B.; Mittal, A.; Kim, S. H., Dependence of sum frequency generation (SFG) spectral features on the mesoscale arrangement of SFG-active crystalline domains interspersed in SFG-inactive matrix: A case study with cellulose in uniaxially aligned control samples and alkali-treated secondary cell walls of plants. *J. Phys. Chem. C* **2017,** *121* (18), 10249-10257.
52. Zhang, T.; Mahgsoudy-Louyeh, S.; Tittmann, B.; Cosgrove, D. J., Visualization of the nanoscale pattern of recently-deposited cellulose microfibrils and matrix materials in never-dried primary walls of the onion epidermis. *Cellulose* **2013,** *21* (2), 853-862.
53. Zhang, T.; Vavylonis, D.; Durachko, D. M.; Cosgrove, D. J., Nanoscale movements of cellulose microfibrils in primary cell walls. *Nat. plants* **2017,** *3* (5), 17056.

54. Kafle, K.; Xi, X.; Lee, C. M.; Tittmann, B. R.; Cosgrove, D. J.; Park, Y. B.; Kim, S. H., Cellulose microfibril orientation in onion (Allium cepa L.) epidermis studied by atomic force microscopy (AFM) and vibrational sum frequency generation (SFG) spectroscopy. *Cellulose* **2014,** *21* (2), 1075-1086.
55. Barnette, A. L.; Lee, C.; Bradley, L. C.; Schreiner, E. P.; Park, Y. B.; Shin, H.; Cosgrove, D. J.; Park, S.; Kim, S. H., Quantification of crystalline cellulose in lignocellulosic biomass using sum frequency generation (SFG) vibration spectroscopy and comparison with other analytical methods. *Carbohydr. Polym.* **2012,** *89* (3), 802-9.
56. Lee, C. M.; Kafle, K.; Belias, D. W.; Park, Y. B.; Glick, R. E.; Haigler, C. H.; Kim, S. H., Comprehensive analysis of cellulose content, crystallinity, and lateral packing in Gossypium hirsutum and Gossypium barbadense cotton fibers using sum frequency generation, infrared and Raman spectroscopy, and X-ray diffraction. *Cellulose* **2015,** *22* (2), 971-989.
57. Nishiyama Y, P. J., Jean B, Heux L *Ordering of cellulose microcrystals dispersed in polar and nonpolar medium*; ESRF: 2006.
58. Barhoumi Meddeb, A.; Chae, I.; Han, A.; Kim, S. H.; Ounaies, Z., Magnetic field effects on cellulose nanocrystal ordering in a non-aqueous solvent. *Cellulose* **2020**.
59. Ogawa, Y.; Lee, C. M.; Nishiyama, Y.; Kim, S. H., Absence of Sum Frequency Generation in Support of Orthorhombic Symmetry of α-Chitin. *Macromolecules* **2016,** *49* (18), 7025-7031.
60. Kong, L.; Lee, C.; Kim, S. H.; Ziegler, G. R., Characterization of starch polymorphic structures using vibrational sum frequency generation spectroscopy. *J. Phys. Chem. B* **2014,** *118* (7), 1775-83.
61. Rocha-Mendoza, I.; Yankelevich, D. R.; Wang, M.; Reiser, K. M.; Frank, C. W.; Knoesen, A., Sum Frequency Vibrational Spectroscopy: The Molecular Origins of the Optical Second-Order Nonlinearity of Collagen. *Biophys. J.* **2007,** *93* (12), 4433-4444.